ELSEVIER

Carbohydrate Polymers 47 (2002) 219–231

Carbohydrate Polymers

www.elsevier.com/locate/carbpol

Prediction of the nonlinear transient and oscillatory rheological behavior of flour suspensions using a strain-separable integral constitutive equation

C.J. Carriere*, A.J. Thomas, G.E. Inglett

Biomaterials Processing Research Unit, National Center for Agricultural Utilization Research, Agricultural Research Service, United States Department of Agriculture, 1815 North University Street, Peoria, IL 61604, USA

Received 29 July 2000; revised 23 December 2000; accepted 29 December 2000

Abstract

The evaluation and development of validated models for the nonlinear viscoelastic (VE) behavior of materials is an important area of research, which has impact on a number of industrial processes including those in the food industry. Various nonlinear VE models have been developed over the years and evaluated for petroleum-based polymers; however, our understanding of the nonlinear VE behavior of biopolymers of industrial import lags our understanding of synthetic polymers. In the work reported herein, the nonlinear VE behaviors of defatted oat flour, oat bran, barley flour, and oat flour suspensions were investigated. The rheological properties were measured using a Rheometrics Series IV controlled-strain rheometer equipped with a cone and plate fixture. The measurements were conducted at 23 ± 0.5°C. The rheological data were interpreted using a strain-separable K-BKZ type (Wagner) model with a damping function evaluated from stress relaxation data. The Wagner model was found to provide an accurate description of the rheological behavior of the suspensions produced from defatted oat flour, barley flour, and oat bran. For suspensions produced from oat flour, the model predictions deviated from the experimental data to a greater degree than the other materials. © 2002 Published by Elsevier Science Ltd.

Keywords: Rheology; Constitutive analysis; Flour; Nonlinear viscoelasticity

1. Introduction

Over the past several years, considerable research efforts have been directed towards understanding the nonlinear viscoelastic (VE) behavior of materials. The investigation of nonlinear VE properties in materials presents a rich field of study. Nonlinear VE properties are of import in a number of diverse industrial processes including extrusion, injection molding, steam-injection cooking, dough mixing, and film tentering. Nonlinear VE properties may be observed in many materials at high strains; however, the effect can also be observed at small strains for many systems such as suspensions and composites (Matsumoto, Hitomi & Onogi, 1975; Russel, 1980; Russel, Saville & Scholwater, 1989; Simhambhatla & Leonov, 1995; Watanabe, Yao, Osaki, Shikata, Niwa & Morishima, 1996, 1997). In many of these systems, the suspended particles form aggregates, which exhibit highly nonlinear VE behavior even at low strains (Matsumoto et al., 1975; Russel, 1980; Russel et al., 1989).

Nonlinear VE behavior is also observed in a number of biological and food systems (Lapasin & Pricl, 1995; Lapasin, Pricl & Tracanneli, 1992). Many biological polymers form weak physical gels, which display nonlinear VE properties similar to those observed in many synthetic polymer-concentrated solutions and melts at high strains or polydisperse systems at low strains (Lapasin & Pricl, 1995; Lapasin et al., 1992). For many biological polymer systems, associations between the various components of a blend or between the biopolymer and the solvent can lead to unexpected nonlinear VE behavior such as multiple stress overshoots during the startup of steady-state shear or regions of shear-thickening behavior. The characterization and understanding of these phenomena in biopolymer systems severely lags our understanding of nonlinear VE behavior in synthetic polymers.

Flours constitute a wide variety of complicated blends of proteins, fats, and carbohydrates. These materials are widely used in the food industry to produce a number of products, most notably, baked goods such as breads. Flours are a major component in bread dough. Dough constitutes an industrially important, highly complicated material that exhibits nonlinear VE behavior at very low strains. Numerous researchers have examined the linear and nonlinear VE properties of dough, but numerous problems remain in

* Corresponding author. Tel.: +1-309-681-6240; fax: +1-309-681-6685.
E-mail address: carriecj@mail.ncaur.usda.gov (C.J. Carriere).

0144-8617/02 - see front matter © 2002 Published by Elsevier Science Ltd.
PII: S0144-8617(01)00165-5

measuring and predicting the behavior of this complicated system (Bagley, Dintzis & Chakrabarti, 1998). Many factors, including processing parameters such as mixing time and procedure as well as water content and temperature affect the rheological properties of prepared dough.

The aim of this present study is to eliminate some of the complications in examining the rheological properties of dough by focusing initially on one of the major components, namely, flour. In the work reported herein, the nonlinear VE properties of suspensions made from flour of four different botanical types are examined. The experimental data are interpreted using a Wagner constitutive model. The Wagner model predictions are compared against experimental data obtained from oscillatory shear, start-up, and cessation of steady-state shear and constant steady shear experiments.

2. Experimental

2.1. Materials

Defatted oat fines (DFOF) were obtained from ConAgra Corporation (Omaha, NE). The DFOF sample was produced from hexane-extracted oat flakes. Oat flour (OF) was obtained from The Quaker Oats Company (Chicago, IL) and was designated as Oat Flour Number 36. Barley flour (BF) was obtained from ConAgra Corporation (Omaha, NE) and was designated as lot number 33320. Oat bran concentrate (OB) was obtained from The Quaker Oats Company (Chicago, IL) and was an experimental air-classified sample. All of the materials were used as-received and were stored in a 0°C walk-in freezer prior to use to prevent degradation. The compositions of the starting materials are listed in Table 1.

2.2. Sample preparation

Samples for the rheological experiments were prepared by dispersing the appropriate flour in deionized water at a concentration of 20% by weight for OB and BF and at 30% by weight for DFOF and OF. The concentrations were not corrected for moisture in the solid material. The suspension was agitated using a Brinkman Polytron homogenizer. Some viscous heating occurred during the mixing process. The mixture was cooled to room temperature and used directly in the experiments. Fresh samples were made daily to ensure that the material had not undergone decomposition. Sample variations typically were within the range of ±10–15%.

2.3. Rheological measurements

Rheological properties were measured using a Rheometrics ARES Series IV controlled-strain rheometer with a cone-and-plate fixture operating under Rheometrics Orchestrator™ Version 6.4.3 software. All the rheological studies were conducted using a 50-mm diameter, 0.0408-rad cone. The rheometer was housed within a constant temperature (23 ± 0.5°C) and humidity (50 ± 2% relative humidity) laboratory. The fits to the experimental data and calculations for the Wagner constitutive model predictions were performed using Mathsoft MathCad 6.0 and Waterloo Maple V software running on a 466-MHz Apple Macintosh G3 computer. Graphical presentations of the data and model predictions were generated using Wavemetrics Igor Pro 3.15 software. Names are necessary to report factually on available data; however, the USDA neither guarantees nor warrants the standard of the product and the use of the name by the USDA implies no approval of the product to the exclusion of others that may also be suitable.

2.4. Constitutive model

The constitutive equation used in this work is the Wagner model, which derives from the K-BKZ equation. The Wagner model may be expressed as (Bernstein, Kearsley & Zapas, 1963; Wagner, 1976, 1978):

$$\underline{\underline{\tau}} = -\int_{-\infty}^{t} m(t-t')h(I_B, II_B)\underline{\underline{B}}(t')\,\mathrm{d}t' \tag{1}$$

where $\underline{\underline{\tau}}$ is the stress dyadic, $\underline{\underline{B}}(t')$ is the Finger strain dyadic, which describes the strain history imparted to the material, $m(t-t')$ is the memory function and $h(I_B, II_B)$ is the damping function, which is expressed in terms of the first and second invariant of the Finger strain dyadic. In simple shear, the damping function becomes a function of the strain γ. Implicit in the presentation of Eq. (1) is the assumption of strain-time factorability. The memory function in Eq. (1) may be expressed as a summation of exponentials:

$$m(t-t') = -\frac{\partial G(t-t')}{\partial t} = \sum_p \frac{G_p}{\tau_p}\,\mathrm{e}^{-(t-t')/\tau_p} \tag{2}$$

where $G(t-t')$ is the stress relaxation modulus and the set G_p and τ_p define the relaxation behavior of the material.

Application of Eq. (1) first requires that the relaxation

Table 1
Composition of flour samples

Material	Moisture	Protein	Lipid	Ash	Crude fiber	β-Glucan	CHO
OB	6.5	18.0	6.6	3.1	3.0	8.6	54.2
OF	11.1	15.3	6.6	2.0	1.3	3.2	60.5
BF	8.4	15.1	5.1	1.7	1.1	19.0	49.6
DOF	6.6	14.7	0.9	1.8	0.8	3.0	72.2

function be determined from the linear VE regime. Once the linear VE range is determined, the damping function can then be calculated from the ratio of the nonlinear stress relaxation modulus $G(\gamma, t - t')$ to the linear stress relaxation modulus $G(t - t')$:

$$h(\gamma) = \frac{G(\gamma, t - t')}{G(t - t')} \tag{3}$$

Many different forms have been advanced for the damping function by Wagner (Eq. (9)), Laun (1978) and Soskey and Winter (1984) to name the most widely used (Eqs. (4)–(6), respectively). These equations may be expressed as

$$h(\gamma) = \mathrm{e}^{-K\gamma} \tag{4}$$

$$h(\gamma) = \frac{1}{1 + a\gamma^b} \tag{5}$$

$$h(\gamma) = K\,\mathrm{e}^{-a_1\gamma} + (1 - K)\,\mathrm{e}^{-a_2\gamma} \tag{6}$$

where γ is the shear strain, and K, a, b, a_1, and a_2 are fitting parameters for the various formulations. For many synthetic polymeric materials, the double exponential equation proposed by Laun has been used extensively to describe the nonlinear VE behavior at large strains. Once a damping function has been selected and the linear VE behavior of the material has been evaluated, the nonlinear behavior of the system can be predicted using Eq. (1).

3. Results and discussion

3.1. Evaluation of linear VE behavior

The effect of shear strain on the measured dynamic storage and loss moduli, G' and G'', for a 20% by weight OB suspension is illustrated in Fig. 1. The linear and nonlinear VE regions are readily evident for the material. At the lowest strains, the data exhibit a slight degree of scatter due to the sensitivity of the rheometer's stress transducer. Below a strain of 1 or 2%, G' is observed to be independent of the applied strain, i.e. linear VE behavior. Above a strain of 2%, the modulus is observed to drop with increasing strain indicating the onset of nonlinear VE behavior. The other flours exhibited similar behavior with nonlinear effects observed to occur at strains greater than 1–2%.

The stress relaxation behavior of OB, OF, DOFOF, and BF suspensions are illustrated in Fig. 2. Strains of 0.1, 0.2, 0.5, 1, 2, 5, 10, 20, 50, 70, and 100% were applied (for clarity, only a limited number of strain levels are displayed for each material in Fig. 2). As the strain level is increased above 1–2%, the absolute value of the stress relaxation modulus is observed to decrease with increasing strain indicating nonlinear VE behavior. Although all of the samples exhibit nonlinear VE behavior, none of the materials displayed any indication of strain hardening at the strain levels investigated. The values of G_p and τ_p were obtained

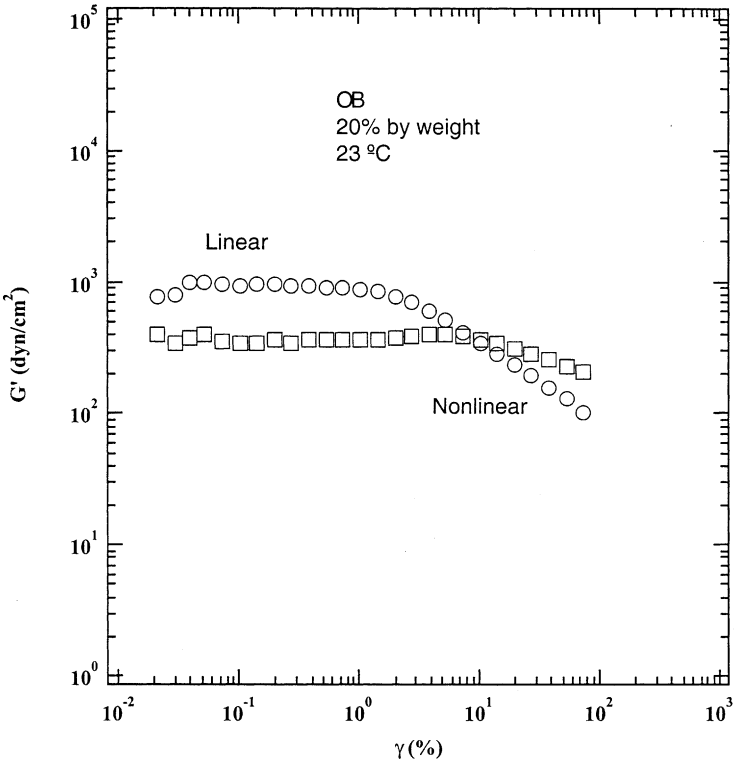

Fig. 1. Effect of shear strain on the dynamic storage and loss moduli, G' and G'', at 1 rad s^{-1} and 23°C for a 20% by weight OB suspension. Nonlinear VE behavior is observed at strains greater than 1–2%.

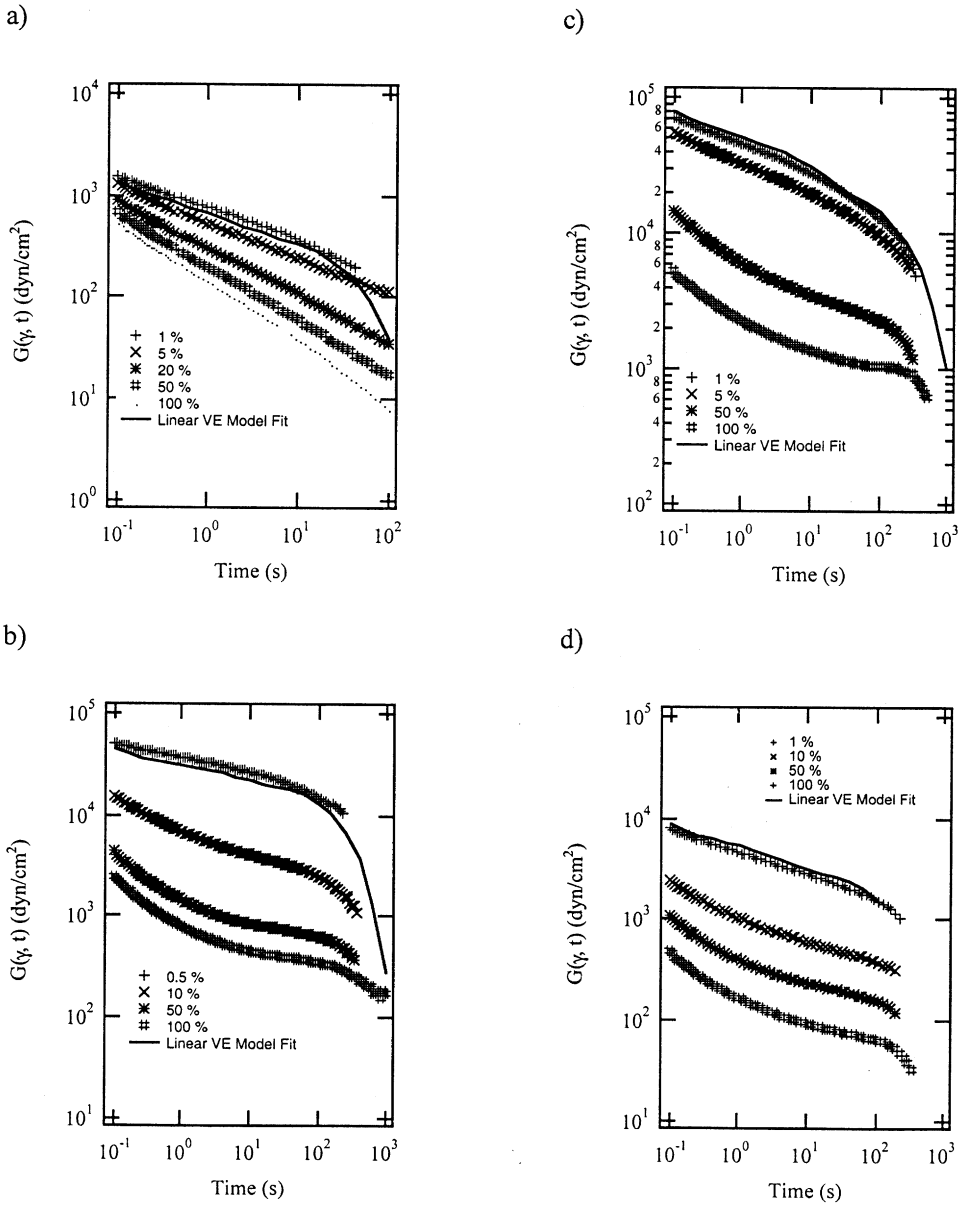

Fig. 2. Stress relaxation behavior for suspensions of (a) OB, (b) OF, (c) DFOF, and (d) BF at 23°C and at various applied strains. Fits to the linear VE regime using Eq. (2) are indicated by solid lines.

by fitting Eq. (2) to the linear stress relaxation data for each of the flour suspensions. The data fits were obtained using the modeling module in the Rheometrics Orchestrator™ Version 6.4.3 software, which uses a nonlinear Levenberg–Marquardt routine. Typically six relaxation times were used to describe the experimental data. The model fits to the linear VE portion of the curves are illustrated in Fig. 2 for each of the suspensions as a solid line. The values for G_p and τ_p for each of the suspensions along with the associated ± one sigma errors are summarized in Table 2.

3.2. Evaluation of the damping function

The damping function in the Wagner model can be determined from the ratio of the nonlinear stress relaxation modulus at a specific strain level to the linear stress relaxation modulus as described above. This procedure was used to evaluate the damping functions for each of the four suspensions. The selection of the appropriate damping function is crucial to developing a constitutive equation that can predict adequately the nonlinear rheological behavior of a material. Three different forms for the damping function were evaluated for each of the flour suspensions, namely those proposed by Wagner, Soskey and Winter, and Laun (Eqs. (4)–(6), respectively). The fits of the various damping functions to the data obtained for the OB suspension is illustrated in Fig. 3. The Wagner formulation predicts a much quicker decrease in the damping function with

Table 2
Fitting parameters for Wagner model of flour suspensions

Material	τ_p	G_p	K	a_1	a_2
OB	0.01±0.001	15 998±1000	0.4±0.03	1.6±0.01	12±0.8
	0.076±0.008	21 320±1200			
	0.58±0.06	8630±200			
	4.46±0.5	3145±60			
	34±3	5250±80			
DFOF	0.01±0.001	2910±200	0.40±0.03	2.1±0.06	24±1
	0.056±0.004	48 140±3000			
	0.328±0.02	17 810±800			
	1.89±0.06	13 200±1000			
	10.8±0.5	21 000±900			
	61.6±2	7200±500			
	350±7	17 400±1000			
BF	0.01±0.001	4700±300	0.14±0.01	1.6±0.01	13±1
	0.056±0.002	7760±400			
	0.32±0.02	1950±200			
	1.75±0.07	1540±100			
	9.77±0.8	1220±100			
	54.6±1	454±20			
	300±5	2180±200			
OF	0.01±0.001	25 700±800	0.045±0.003	1.9±0.1	16±1
	0.075±0.003	29 800±600			
	0.56±0.03	6830±300			
	4.2±0.07	12 200±900			
	31.4±0.9	2320±200			
	235±4	23 500±2000			

increasing strain in the nonlinear VE regime than is observed in the experimental data. Both the Soskey–Winter and the Laun equations provide an adequate description of the experimentally obtained damping function. Similar observations were made for OF, DFOF, and BF suspensions.

In this work, the Laun damping function was chosen to describe the effects on nonlinearity of the VE functions. Use of the Soskey–Winter damping function provided predictive results that were indistinguishable from those obtained using the Laun damping function. The values for K, a_1, and a_2 obtained for the Laun damping function on each of the flour suspensions along with the associated ± one sigma errors are summarized in Table 2. The values of a_2 in the fits of the Laun damping function were in the range of 12–24 indicating the marked strain softening and limited strain regime of the linear VE behavior observed for these suspensions.(Gallegos, Pedrero, Madiedo & Franco, 2000).

3.3. Prediction of nonlinear rheological behavior

3.3.1. Successive start-up of steady-state shear

The results of a series of start-up of steady-state shear experiments on OB, OF, DFOF, and BF suspensions are illustrated in Fig. 4. The applied shear rates ranged from 0.01 to 10 s^{-1}. Each of the shear rates was applied to the sample for 100 s. At the end of the 100 s time period, the shear rate was increased to the next level without allowing the sample to relax. The shear stress growth coefficient, $\eta^+(\dot{\gamma},t)$, is observed to decrease with increasing shear rate, $\dot{\gamma}$. For all of the suspensions, $\eta^+(\dot{\gamma},t)$ is observed to rise rapidly to a stable plateau at all of the applied shear rates. For DFOF at 0.1 and 1 s^{-1}, OF at 0.1 s^{-1}, and BF at 0.1 s^{-1}, stress overshoot behavior is observed. For OB, stress overshoot behavior is not observed at any of the applied shear rates used in this study.

For the start-up of steady-state shear experiment, the Wagner model may be rewritten as:

$$\eta^+(\dot{\gamma},t) = \int_0^t G(s)\left[s\frac{\partial h(s)}{\partial s} + h(s)\right]\mathrm{d}s \tag{7}$$

where $G(s)$ and $h(s)$ are defined in Eqs. (2) and (6), respectively. The prediction of the Wagner model for linear VE behavior may be calculated using Eq. (7) with $h(s) = 1$. The linear and nonlinear VE behavior as predicted by the Wagner model for each of the suspensions are displayed in Fig. 4 as dashed and solid lines, respectively. For each of the suspensions, the linear VE Wagner model over-predicts the stress growth functions at all of the shear rates. For OB and DFOF, the nonlinear VE Wagner model over-predicts the stress growth functions at a shear rate of 0.01 s^{-1}. At a shear rate of 0.1 s^{-1}, the model correctly predicts the stress overshoots observed for OF, DFOF, and BF, and predicts the final plateau value for the stress growth function to be better than ±20%. The model also predicts stress overshoots at 0.1 s^{-1} for OB, which was not observed experimentally. At shear rates of 1 and 10 s^{-1}, the model

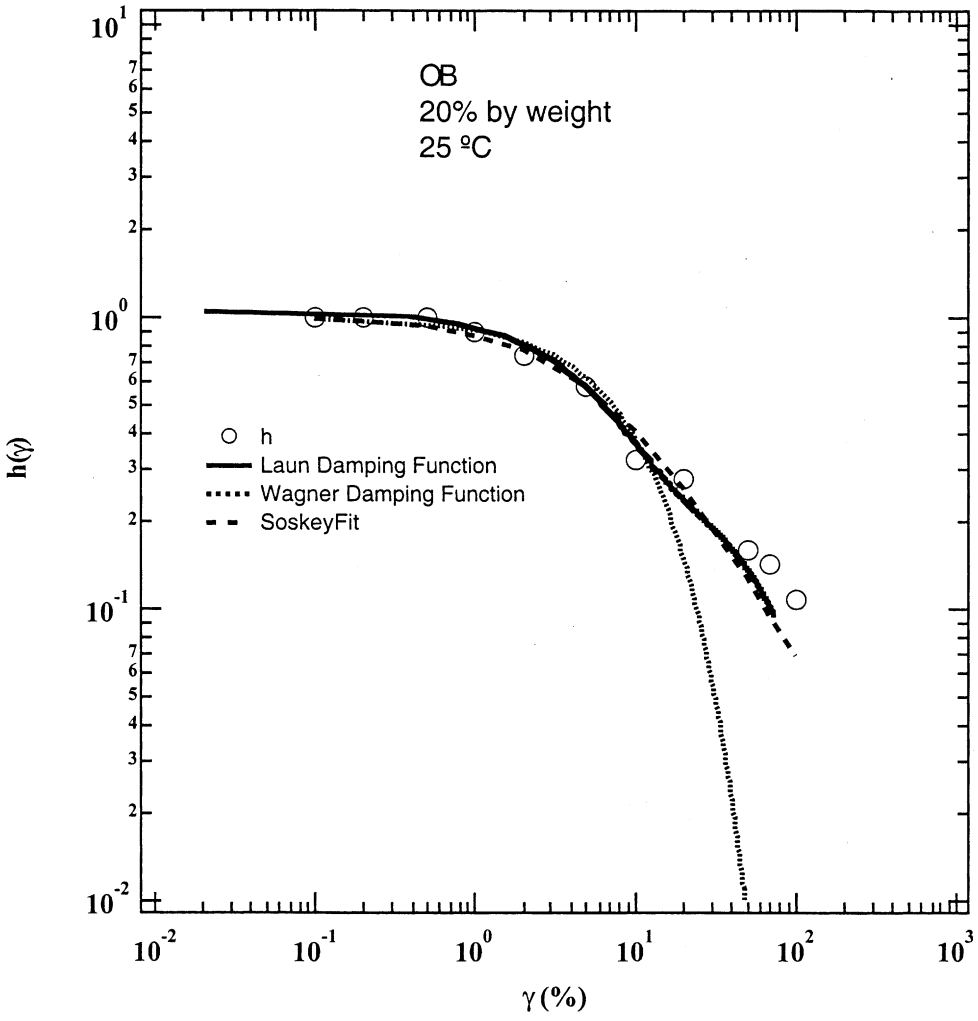

Fig. 3. Evaluation of the damping function for a 20% by weight OB suspension at 23°C. The best fits to the experimental data for the damping functions proposed by Wagner, Soskey–Winter, and Laun (Eqs. (4), (5), and (6), respectively) are displayed.

correctly predicts the value for the stress growth function for OB. For DFOF at 10 s^{-1}, the model under-predicts the value for the stress growth function indicating that the damping function for DFOF is imparting too large of a value for the strain build-up in the sample. For BF, the nonlinear VE Wagner model provides predictions for the stress growth function to better than ±15% at 0.01, 0.1, and 1 s^{-1}. At 10 s^{-1}, the model under-predicts the value for the stress growth function for BF again indicating that the damping function is overestimating the strain build-up in the sample. For OF, the Wagner model under-predicts the observed stress growth function data at all of the shear rates.

3.3.2. Steady-shear rate sweep

The results of a steady-shear rate sweep experiments on OB, OF, DFOF, and BF suspensions are illustrated in Fig. 5. The applied shear rate ranged from 0.01 to nearly 1000 s^{-1}. OB, DFOF, and BF all exhibited shear-thinning behavior across the entire shear rate range studied. OF exhibited a region of shear thinning from 10^{-2} to 10 s^{-1}, which was followed by a region of more moderate shear thinning from 10 to 30 s^{-1}. At shear rates above 30 s^{-1}, OF again displayed shear-thinning behavior similar to that exhibited below shear rates of 10 s^{-1}. For DFOF, at shear rates greater than 20 s^{-1}, the data exhibits a good deal of scatter due to slight extrusion of the sample from the cone and plate geometry. This problem was not observed for the other suspensions. None of the suspensions exhibited a zero-shear viscosity at the lowest shear rates used in this study. Lower shear rates were not accessible with our rheometer for these samples due to limitations in the torque resolution.

The steady-shear rate sweep data for each of the suspensions were fitted to a power law model, i.e. $\eta(\dot{\gamma}) = B\dot{\gamma}^m$ where B and m are model constants. The results of the power law model fits along with the associated ± one sigma errors are summarized in Table 3. The values for m range from -0.609 ± 0.009 for OB to -0.844 ± 0.003 for DFOF. The values obtained for m all indicate shear-thinning behavior and are in the range typically observed for shear-thinning fluids. It should be noted that the power law model

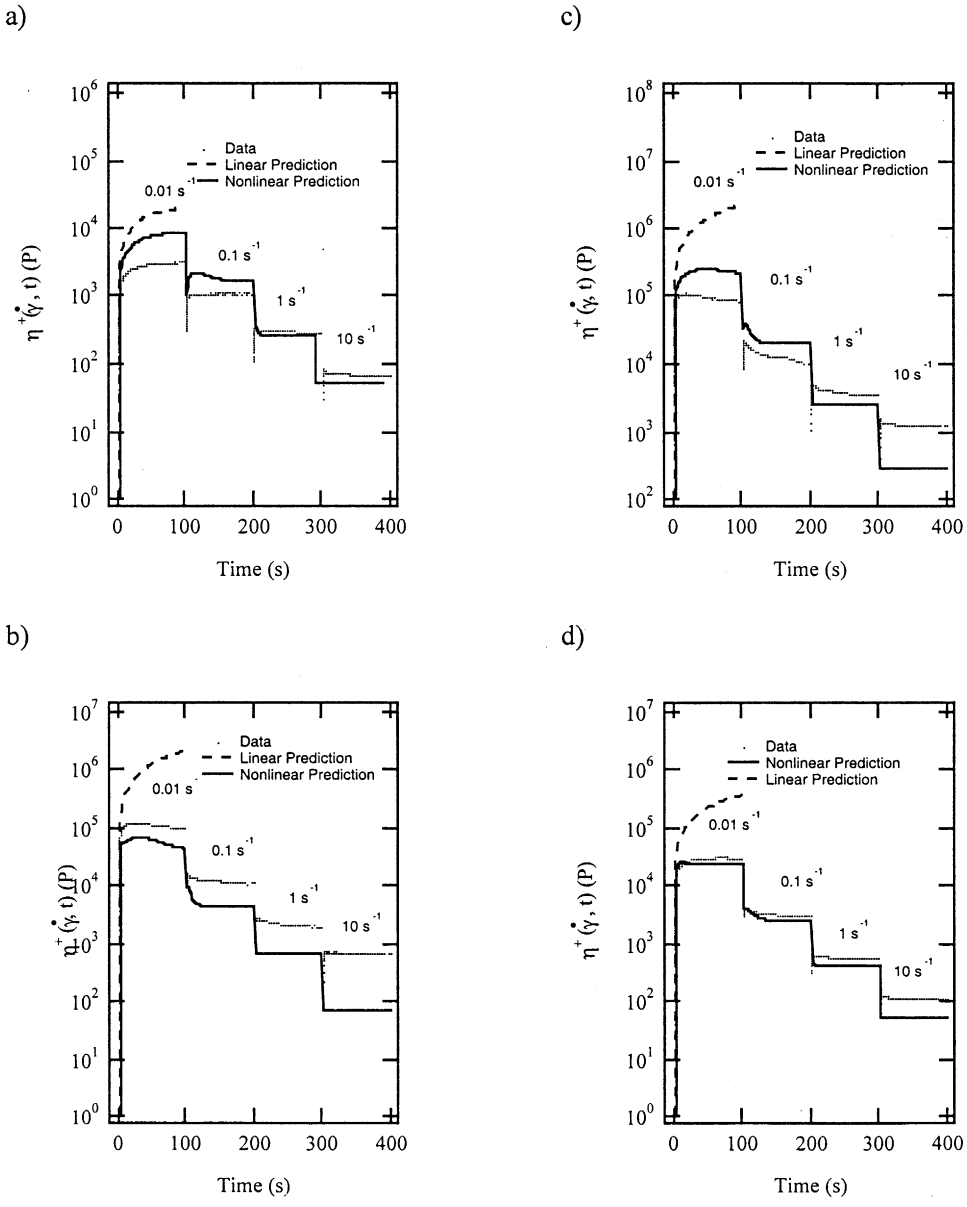

Fig. 4. The effect of shear rate and time on the stress growth coefficient obtained at 23°C for suspensions of (a) OB, (b) OF, (c) DFOF, and (d) BF. The predictions of the linear and nonlinear VE Wagner model are illustrated in the figure with a solid and dotted line, respectively.

parameters listed for OF were evaluated prior to the onset of the change in the shear-thinning behavior.

For steady shear rate sweep experiments, the Wagner model at any shear rate may be rewritten as:

$$\eta(\dot{\gamma}) = \int_0^{t_{meas}} G(s)\left[s\frac{\partial h(s)}{\partial s} + h(s)\right] ds \quad (8)$$

where $\eta(\dot{\gamma})$ is the steady shear viscosity calculated at a shear rate of $\dot{\gamma}$, and t_{meas} is the time of measurement at each shear rate, which for these experiments was 12 s. For linear VE behavior, with $h(s) = 1$, Eq. (8) yields the zero-shear viscosity. The predictions of the Wagner model are presented in Fig. 5 as solid (nonlinear VE) and dotted (linear VE) lines. For OB, DFOF, and BF, the model predictions for the nonlinear VE behavior yield reasonable agreement with the measured magnitudes of the shear viscosity across the shear rate range studied. For OF, the model did not predict the observed change in the shear-thinning behavior. This is due to the absence of shear hardening observed in the stress relaxation experiments for OF, which were used to determine the damping function. The deviation between the model predictions and the experimental data are greatest at the higher shear rates for OF due to the presence of the change in the character of the shear-thinning behavior starting at 10 s^{-1}. None of the experimental data for the suspensions reached a zero-shear viscosity value, so the predictions for this material function could not be evaluated; however, none of the experimental data exceeded the

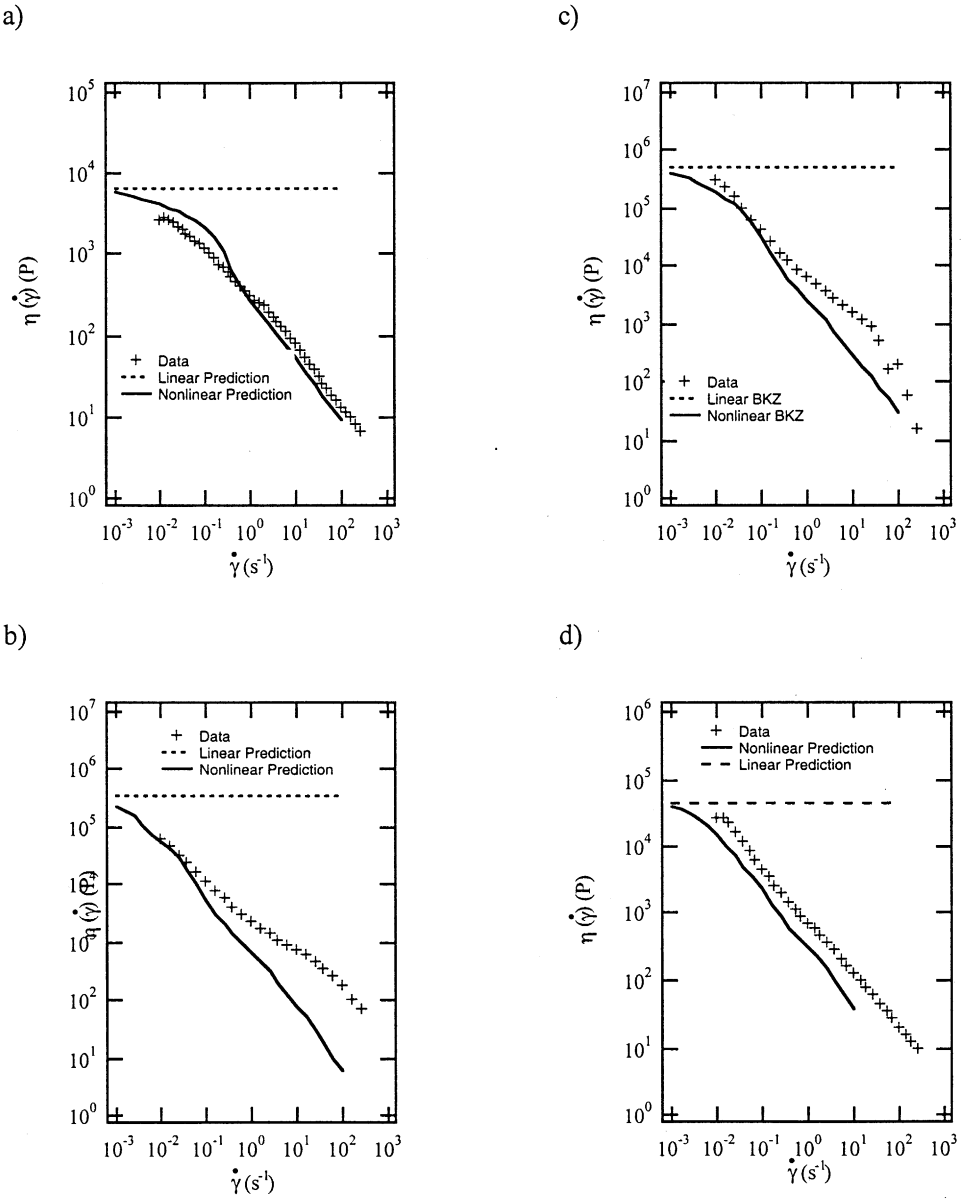

Fig. 5. The effect of shear rate on the steady shear viscosity obtained at 23°C for suspensions of (a) OB, (b) OF, (c) DFOF, and (d) BF. The predictions of the nonlinear and linear Wagner model are illustrated in the figure with solid and dotted lines, respectively.

Table 3
Power law fitting parameters for flour suspensions

Material	B	m
OB	2.427±0.012	−0.609±0.009
OF[a]	3.333±0.007	−0.736±0.006
DFOF	3.834±0.004	−0.844±0.003
BF	2.891±0.007	−0.792±0.005

[a] OF evaluated at shear rates below 10 s^{-1}.

calculated zero-shear viscosity, thus the model predictions for the zero-shear viscosity may be reasonable.

3.3.3. Oscillatory shear flow

The results of oscillatory shear flow experiments on OB, OF, DFOF, and BF suspensions are illustrated in Fig. 6. The applied frequency ranged from 0.1 to 100 rad s^{-1}. For each of the suspensions, the effect of applied strain on the storage modulus, $G'(\gamma, \omega)$, is displayed. For each of the suspensions, the storage modulus is observed to decrease with increasing applied strain indicating nonlinear VE behavior. For OB, DFOF, and BF, $G'(\gamma, \omega)$ decreases monotonically with decreasing frequency as is expected for shear-thinning materials. The OF suspension at a strain of 10% displays a

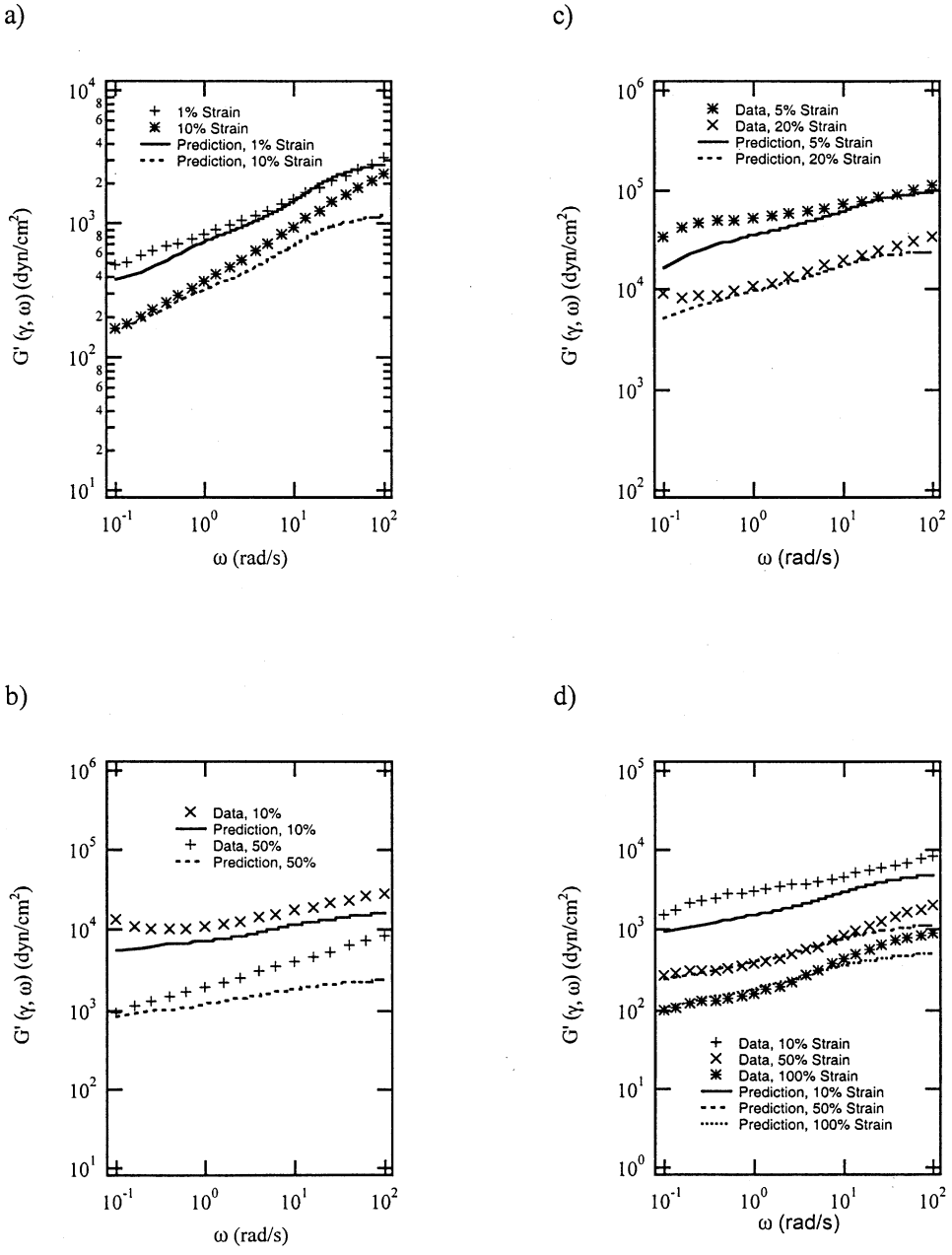

Fig. 6. The effects of frequency and strain on the dynamic storage modulus obtained at 23°C for suspensions of (a) OB, (b) OF, (c) DFOF, and (d) BF. The predictions of the nonlinear and linear Wagner model are illustrated in the figure with solid and dotted lines, respectively.

plateau at low frequencies that is not observed for the other suspensions. This plateau could be indicative of some potential aggregation or other temporary association in the sample.

For the oscillatory shear flow experiment, the Wagner model may be recast as

$$\sigma'(\gamma,\omega) + j\sigma''(\gamma,\omega) = -\int_{-\infty}^{t} m(t-t')h(\gamma)\gamma_0\, e^{j\omega t'}\, dt' \quad (9)$$

where $\sigma'(\gamma,\omega)$, and $\sigma''(\gamma,\omega)$ are the real and imaginary components of the oscillatory shear stress, ω is the angular frequency of the deformation, γ_0 is the peak amplitude of the strain, and $j = \sqrt{-1}$. The storage and loss moduli can be calculated from the real and imaginary components of the stress using $G'(\gamma,\omega) = \sigma'(\gamma,\omega)/\gamma_0$, and $G''(\gamma,\omega) = \sigma''(\gamma,\omega)/\gamma_0$, respectively.

The predictions of the Wagner model for the various suspensions under oscillatory shear flow are illustrated in Fig. 6. For OB, DFOF, and BF, the Wagner model correctly predicts the magnitude of the storage modulus with varying strain level. For DFOF, the model predicts the frequency dependence of the storage modulus over the frequency range of 0.1–100 rad s^{-1}. For OB and BF, deviations of the data from the model predictions are observed at the

higher frequencies. For OF, the deviations between the model predictions and the experimental data are greater than for the other materials. In addition, for OF, the model does not accurately predict the observed frequency dependence of the storage modulus. These deviations are probably due to overestimates of the effective strain during the deformation from the damping function. For OF, the deviations between the model predictions and the experimental data are also probably affected by the lack of strain hardening observed in the stress relaxation experiments. The lack of observed strain hardening also affected the ability of the model to predict the change in the shear-thinning behavior of OF during the steady-shear rate sweep experiments.

3.3.4. Cessation of steady-state shear flow

The results of a series of start-up and cessation of steady-state shear flow experiments for OB, OF, DFOF, and BF suspensions are illustrated in Fig. 7. The experiments were conducted by applying a constant shear to the sample at a specified shear rate for 100 s, then stopping the shear and recording the response of the material for 100 s. The procedure was then repeated for other shear rates of interest. At a shear rate of 0.01 s^{-1}, the experimental data for each of the suspensions is observed to rise rapidly to a stable plateau with no evidence of stress overshoot. After the shear was halted, the shear stress is observed to drop rapidly from the peak value. Upon the inception of an applied shear rate of

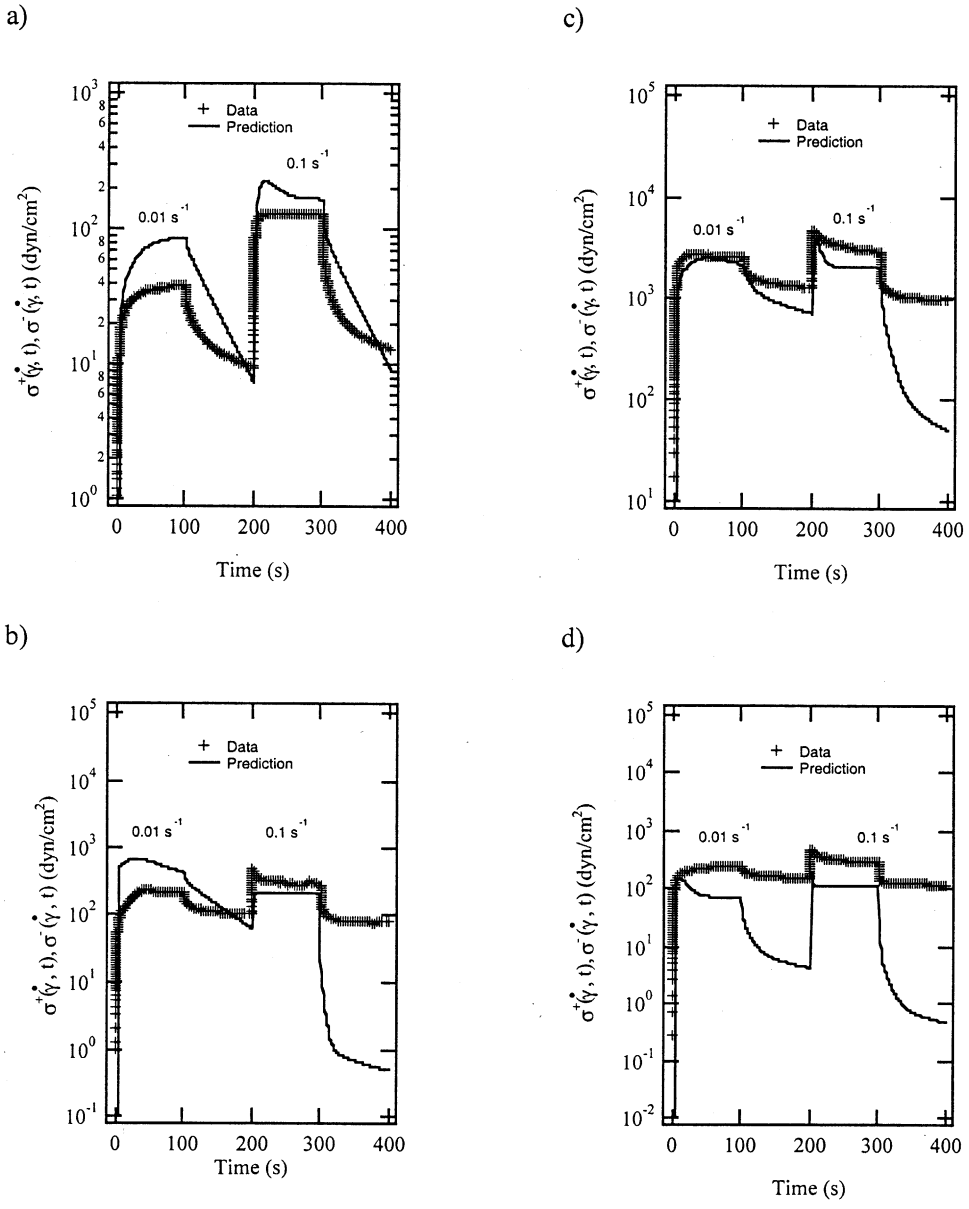

Fig. 7. The effect of shear rate and time on the shear stress growth and decay functions obtained at 23°C for suspensions of (a) OB, (b) OF, (c) DFOF, and (d) BF during start-up and cessation of steady-state shear flow experiments. The predictions of the linear and nonlinear VE Wagner model are illustrated in the figure with a solid and dotted line, respectively.

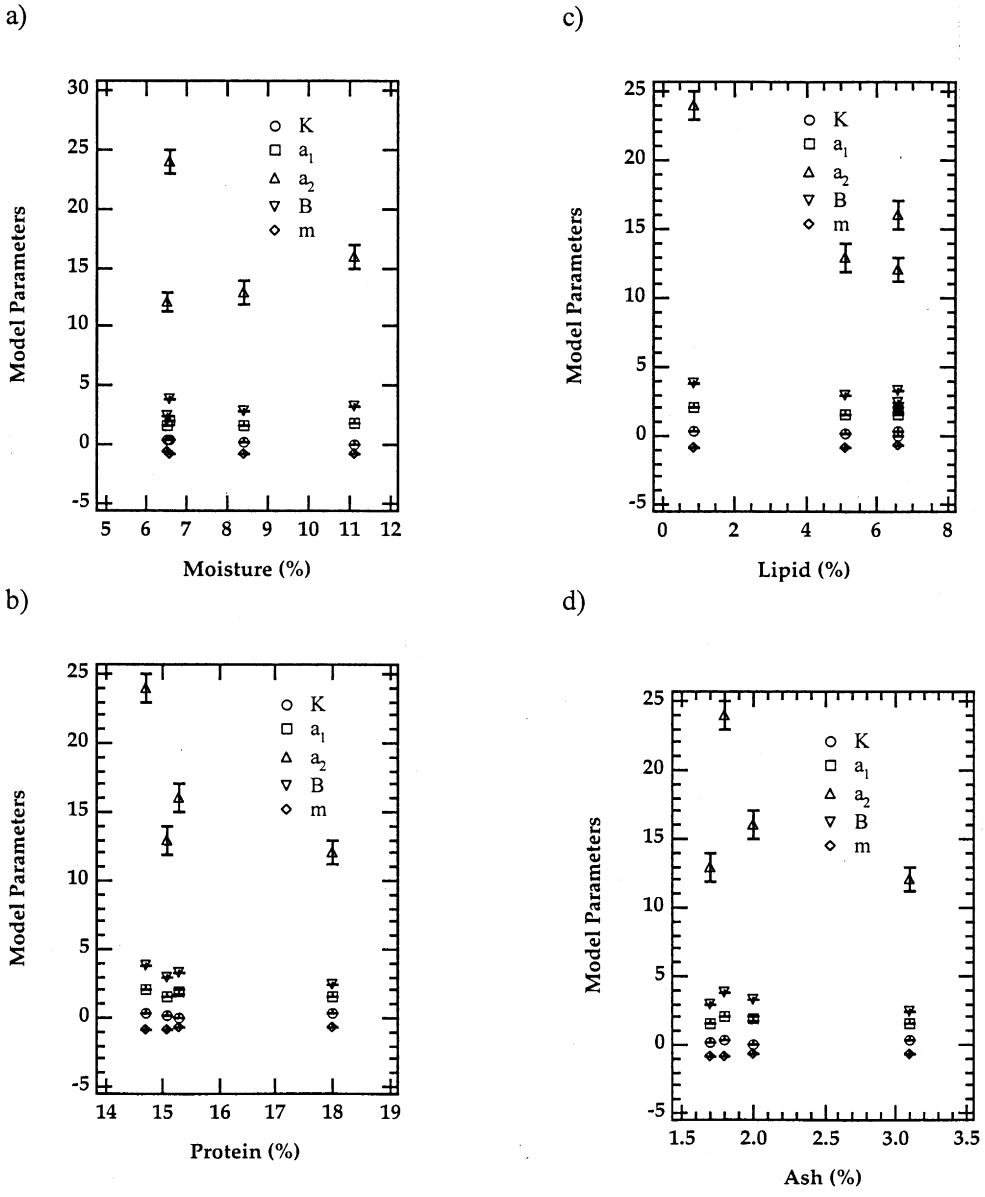

Fig. 8. Effects of (a) moisture, (b) protein, (c) lipid, (d) ash, (e) crude fiber, (f) β-glucan, and (g) total carbohydrate content on the Wagner and power law model parameters used to fit the various flour suspensions.

0.1 s^{-1}, the shear stress is again observed to rise rapidly to a stable plateau and in the case of DFOF, BF, and OF, stress overshoot behavior is observed. After the applied shear rate was stopped, the shear stress is again observed to decrease rapidly from its peak value.

For cessation of steady-state shear flow, the Wagner model may be written as

$$\sigma^{-}(\dot{\gamma},t) = \dot{\gamma}_{\text{cess}} \int_{t}^{t_{\text{cess}}+t} G(s)\left[(s-t)\frac{\partial h(s)}{\partial s} + h(s)\right] \mathrm{d}s \quad (10)$$

where $\sigma^{-}(\dot{\gamma},t)$ is the shear stress decay function, $\dot{\gamma}_{\text{cess}}$ the shear rate, which is applied to sample prior to cessation, and t_{cess} the time the shear rate applied prior to cessation. The shear stress growth function predicted by the Wagner model during start-up of steady-state shear may be obtained from the shear stress growth coefficient given by Eq. (7) using $\sigma^{+}(\dot{\gamma},t) = \eta^{+}(\dot{\gamma},t)\dot{\gamma}_{\text{cess}}$.

The predictions using the Wagner model for the start-up and cessation of steady-state shear flow are illustrated in Fig. 7. For all of the suspensions, the model predictions for the start-up of steady-state flow data have been discussed above. For OB, the Wagner model applied to the cessation of steady-state shear stress at both shear rates investigated predicted the immediate drop in the shear stress after the cessation of steady-state shear flow; however, the experimental data decays faster than the model predictions. For OF, the model predicted the drop in shear stress after the cessation of steady-state shear, but the model predicted a more rapid decay of the stress than was observed experimentally at both of the shear rates. For DFOF, the model

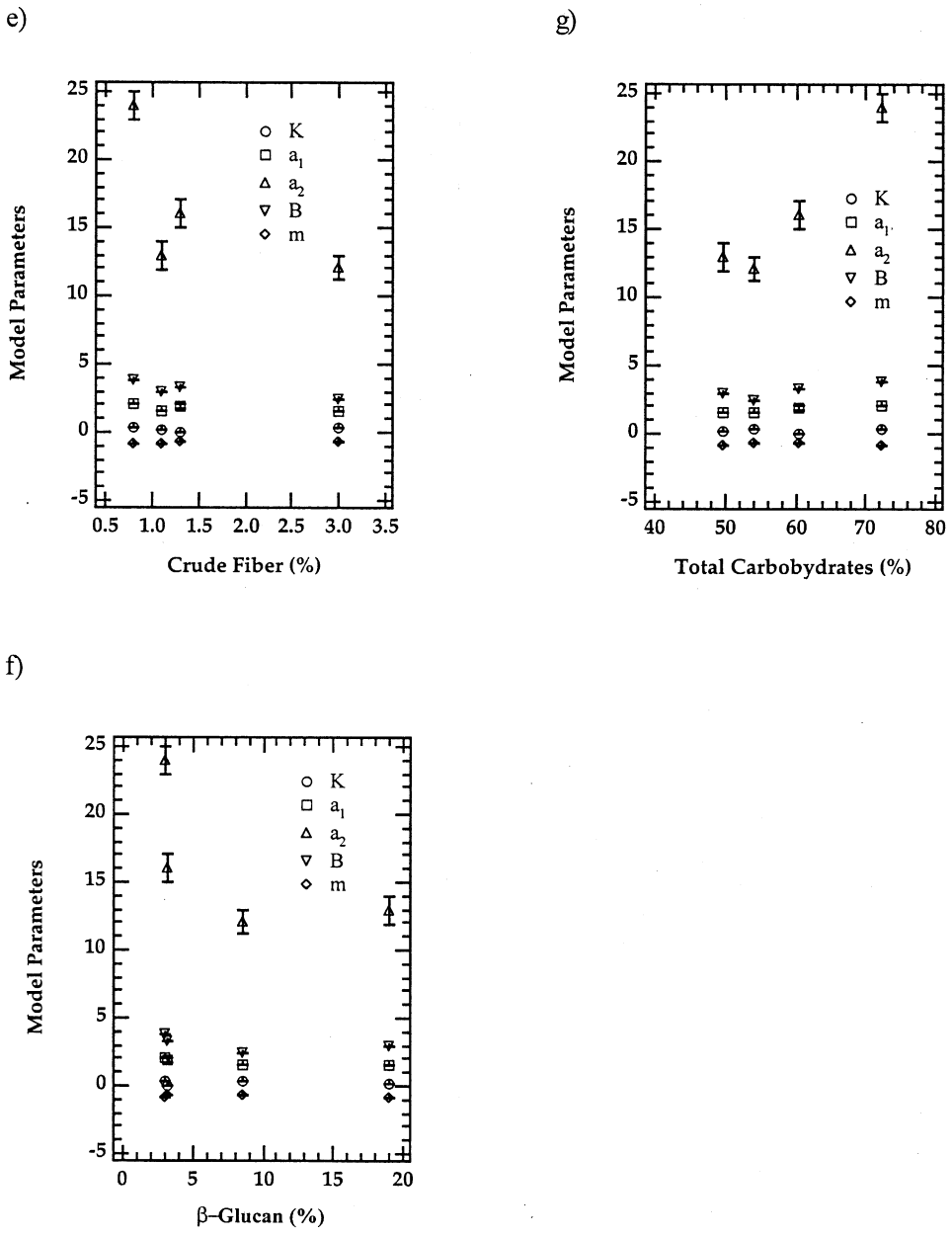

Fig. 8. (*continued*)

again correctly predicts the rapid drop in the shear stress after the cessation of steady-state shear flow, but the model predicts a more rapid drop in the shear stress at higher shear rates than is observed experimentally. These results would indicate that the damping function is over-estimating the build-up of shear stress in both OF and DFOF samples. For BF, the Wagner model under-predicts the absolute value of the shear stress during the cessation experiment as well predicting a quicker drop in the shear stress upon cessation of the applied shear. This result indicates that the damping function for BF is imparting a greater degree of strain build-up in the sample than is actually occurring.

3.4. Effect of flour composition on the VE model parameters

The effect of flour composition on the linear VE model parameters (Eq. (2)), namely, the longest relaxation time, the initial modulus constant associated with the shortest relaxation time, and the modulus constant associated with the longest relaxation time was evaluated (data not displayed). The longest relaxation time was found to decrease systematically with increasing amounts of crude fiber, ash, and protein. The longest relaxation time constant corresponds to short-range motions and interactions in the material. From the data, it is evident that the crude fiber, ash, and proteins in the flours largely dominate the local confor-

mational dynamics. The modulus constants associated with the initial and longest relaxation times were found to increase with increasing total carbohydrate levels. Interestingly, none of the linear VE model parameters displayed any dependence on the β-glucan level in the flours.

The effects of moisture, protein, lipid, ash, crude fiber, β-glucan, and total carbohydrate content on the damping function (Eq. (6)) and power law model parameters are illustrated in Fig. 8 for each of the flour suspensions. As is evident from the figure, the power law model parameters (B and m) did not display any dependence on the compositions of the various flours. The damping function parameter a_2 exhibited an apparent dependence on both the amount of crude fiber and total carbohydrate content as well as a slight dependence on the β-glucan content. The major components in the flours that were controlling the linear VE behavior also appear to control the nonlinear VE behavior as well. The values of the damping function parameters K and a_1 were independent of the flour's composition.

4. Conclusions

The nonlinear VE behavior of DFOF, OB, BF, and OF suspensions made in deionized water were characterized. The DFOF, OB, and BF suspensions were found to exhibit shear-thinning behavior with nonlinear VE behavior evidenced at strains above 1%. For OF, a change in the character of the shear-thinning behavior was found starting at a shear rate of 10 s^{-1}. The linear and nonlinear VE performance of the suspensions was analyzed using a Wagner integral constitutive model. The damping function used in the model was evaluated from stress relaxation data. The Wagner model was used to predict the performance of the various flour suspensions under difference shear deformations including steady-state shear, start-up and cessation of steady-state shear, and oscillatory shear. The Wagner model was found to provide an adequate description of the nonlinear VE behavior of the suspensions produced from DFOF, OB, and BF in the different shear deformations. For OF suspensions, the model predictions deviated from the experimental data to a greater degree than the other suspensions. The model was unable to predict the change in the shear-thinning behavior of the OF suspension due to the lack of observed stress hardening in the nonlinear stress relaxation behavior.

The total carbohydrate and crude fiber content of the flours were found to affect both the linear and nonlinear VE model parameters. In addition, the linear VE model parameters also displayed dependence on amount of ash and protein in the flours. The β-glucan content in the flours was found to have a slight effect on one of the damping function parameters in the nonlinear VE model.

Acknowledgements

The authors thank Dr E. B. Bagley, Dr R. L. Sammler, and Dr J. A. Byars for helpful discussions and encouragement throughout the course of this work. The work was supported by the United States Department of Agriculture, Agricultural Research Service.

References

Bagley, E. B., Dintzis, F. R., & Chakrabarti, S. (1998). Experimental and conceptual problems in the rheological characterization of wheat flour doughs. *Rheologica Acta*, *37*, 556–565.

Bernstein, B., Kearsley, E. A., & Zapas, L. J. (1963). A theory of stress relaxation with finite strain. *Transactions of the Society of Rheology*, *7*, 391–410.

Gallegos, C., Pedrero, E. M., Madiedo, J. M., & Franco, J. M. (2000). Nonlinear viscoelasticity and microstructure of o/w emulsions. In P. Fischer, I. Marti & E. J. Windhab, *Proceedings of the 2nd International Symposium on Food Rheology and Structure* (pp. 57–62). Lappersdorf, Germany: Kerschensteiner Verlag.

Lapasin, R., & Pricl, S. (1995). *Rheology of industrial polysaccharides*, London: Chapman & Hall.

Lapasin, R., Pricl, S., & Tracanneli, P. (1992). Different behavior of concentrated polysaccharide systems in large-amplitude oscillatory fields. *Rheologica Acta*, *31*, 374–380.

Laun, H. M. (1978). Description of the nonlinear shear behavior of a low density polyethylene by means of an experimentally determined strain dependent memory function. *Rheologica Acta*, *17*, 1–15.

Matsumoto, T., Hitomi, C., & Onogi, S. (1975). Rheological properties of disperse systems of spherical particles in polystyrene solutions at long time scales. *Transactions of the Society of Rheology*, *19*, 541–555.

Russel, W. B. (1980). Review of the role of colloidal forces in the rheology of suspensions. *Journal of Rheology*, *24*, 287–314.

Russel, W. B., Saville, D. A., & Scholwater, W. R. (1989). *Colloid dispersion*, Cambridge, UK: Cambridge University Press.

Simhambhatla, M., & Leonov, A. I. (1995). On the rheological modeling of filled polymers with particle–matrix interactions. *Rheologica Acta*, *34*, 329–338.

Soskey, P. R., & Winter, H. H. (1984). Large step strain experiments with parallel-disk rotational rheometers. *Journal of Rheology*, *28*, 625–645.

Wagner, M. H. (1976). Analysis of time-dependent non-linear stress-growth data for shear and elongational flow of low-density branched polyethylene melt. *Rheologica Acta*, *15*, 136–142.

Wagner, M. H. (1978). A constitutive analysis of uniaxial elongational flow data of a low-density polyethylene melt. *Journal of Non-Newtonian Fluid Mechanics*, *4*, 39–55.

Watanabe, H., Yao, M. -L., Osaki, K., Shikata, T., Niwa, H., & Morishima, Y. (1996). Nonlinear rheological behavior of a concentrated spherical silica suspension. *Rheologica Acta*, *35*, 433–445.

Watanabe, H., Yao, M. -L., Osaki, K., Shikata, T., Niwa, H., & Morishima, Y. (1997). Nonlinear rheology of a concentrated spherical silica suspension. 2. Role of strain in shear-thickening. *Rheologica Acta*, *36*, 524–533.